Biosensors and Bioelectronics 29 (2011) 53–59

Contents lists available at ScienceDirect

Biosensors and Bioelectronics

journal homepage: www.elsevier.com/locate/bios

Nano polyurethane-assisted ultrasensitive biodetection of H_2O_2 over immobilized Microperoxidase-11

Zhenping Chen, Dongmei Sun*, Yiming Zhou, Jiayue Zhao, Tianhong Lu, Xiaohua Huang*, Chenxin Cai, Jian Shen

Jiangsu Key Laboratory of New Power Batteries, Jiangsu Key Laboratory of Biofunctional Materials, College of Chemistry and Materials Science, Nanjing Normal University, Nanjing 210046, PR China

ARTICLE INFO

Article history:
Received 10 May 2011
Received in revised form 25 July 2011
Accepted 26 July 2011
Available online 2 August 2011

Keywords:
Biosensor
Nano-polyurethane
Microperoxidase-11
Hydrogen peroxide

ABSTRACT

Nanostructured polyurethane (PU) synthesized by an emulsion polymerization with narrow size distribution was employed for the first time directly as a novel matrix for enzyme immobilization to develop sensitively amperometric biosensors. When Microperoxidase-11 (MP-11) was selected as a model protein, the resulting hydrogen peroxide (H_2O_2) biosensor exhibited improved sensitivity of 29.6 μA mM^{-1} cm^{-2} with quite good response time of (1.3 ± 0.4) s and remarkable limit of detection as low as 10 pM (S/N 3) over existing protocols. A linear calibration curve for hydrogen peroxide was obtained up to 1.3 μM under the optimized conditions with a relative low calculated Michaelis–Menten constant (K_M^{app}) (1.87 ± 0.05) μM, which indicated the enhanced enzymatic affinity of MP-11 to H_2O_2 via PU. The possible interferents had negligible effect on the response current and time of the prepared biosensor. Results suggest that the PU nanoparticles (PU-NPs) with good biocompatibility and sufficient interfacial adhesion hold promise as an attractive support material for construction of ultrasensitive amperometric biosensor.

1. Introduction

Hydrogen peroxide (H_2O_2) present in small as a natural by-product of oxidative metabolism, plays versatile biological roles in vivo (Niethammer et al., 2009; Poole and Nelson, 2008; Schraufstatter et al., 1986). It has been recognized that low levels of H_2O_2 can function as a second messenger signal in cell proliferation, differentiation and migration which is corresponding to the states of some human diseases such as diabetes, cancer and ageing, though it will cause oxidative damage to protein, DNA and lipids at elevated levels (Rhee, 2006). In addition, the measurement of H_2O_2 is known as the basis of the quantitative assay of some enzyme activity, biologically important substrates including glucose and enzyme-linked immunoassay (Katz and Willner, 1996; Mir et al., 2008; Wilson and Hu, 2000; Yu et al., 2003). Therefore, a highly sensitive detection of small quantities of hydrogen peroxide is of great importance for providing fundamental information in a variety of practical applications.

Much efforts have been made to create a fast and accurate determination of H_2O_2 based on titrimetric (Klassen et al., 1994), fluorescent (Dickinson and Chang, 2008), phosphorescent (Shu et al., 2007), chemiluminescent (Yuan and Shiller, 1999), UV–vis spectrophotometric (Lo and Chu, 2003), and electrochemical techniques (Chen et al., 2007; Katz and Willner, 1997; Kulys and Tetianec, 2006; Mazzei et al., 2008; Munge et al., 2009; Patolsky et al., 1999). Among these, the electroanalytical methods especially via biosensors over immobilized peroxidase such as Microperoxidase-11 (MP-11) (Katz and Willner, 1997), horseradish peroxidase (HRP) (Munge et al., 2009) and hemoglobin (Hb) (Chen et al., 2007), have fosted their widespread application due to their rapid response time, relative simplicity and high versatility, although not as sensitive as optical detector. Recent work from Lyon and Stevenson (2006) offered much lower H_2O_2 detection limits of 2 nM by a chemically activated Amplex Red-mediated biosensor in concert with microelectrode square wave voltammetry. The amount of H_2O_2 was quantified via the electro-reduction of the on-line produced mediator resorufin from redox-inactive Amplex Red in the presence of immobilized HRP. Apparently, the unmodified working electrode was susceptible to fouling due to the adsorption of the soluble resorufin/dihydroresorufin, which led to extra interference and bad operational stability. Our interest in this paper is trying to develop a novel H_2O_2 electrochemical biosensor, which combines extreme sensitivity and long-term stability, as well as the ease in fabrication and miniaturization.

* Corresponding authors. Tel.: +86 25 85891651.
E-mail addresses: sundongmei@njnu.edu.cn (D. Sun), wxxhhuang@yahoo.com (X. Huang).

0956-5663/$ – see front matter © 2011 Elsevier B.V. All rights reserved.
doi:10.1016/j.bios.2011.07.065

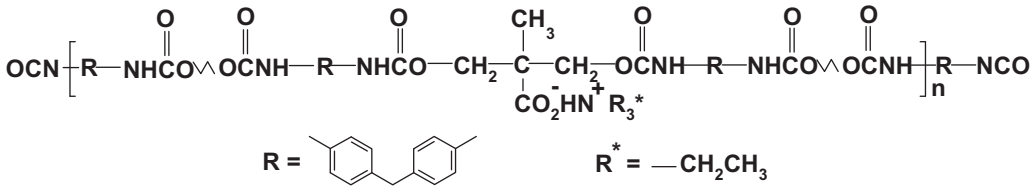

Scheme 1. Chemical structure of the prepared PU.

Polyurethanes are considered as an attractive support material for enzyme immobilization because of their good biocompatibility, desirable mechanical strength, tunable morphology and controllable functionality (Bil et al., 2010; Hood et al., 2010; Koepsel and Russell, 2003; Phadtare et al., 2003; Wang et al., 2002; Xu et al., 2010). Liu et al. (2007) immobilized Hb to the polyurethane elastomer film mixed with multiwalled carbon nanotubes (MWNTs) and developed a well-performed nitrite sensor. The addition of MWNTs is to improve the permeability and conductivity of the relatively compact PU layer. On the other hand, MWNTs is known for the adverse affect on the bioactivity of the linked enzyme because of its toxicity (Deka et al., 2010), which was also observed for colloidal gold (Jiang et al., 2005). In this work, we demonstrate for the first time the immobilization of MP-11 directly on nanostructured polyurethane (PU, mean diameter 50 nm, Scheme 1) without purposely added doping material and electron mediators. Taking advantage of the large surface-to-volume ratio and the increased surface activity of nanoparticles, the immobilized MP-11 not only retains its bioactivity but also shows an excellent electrochemical behavior with a high affinity for H_2O_2 reduction, resulting in a novel H_2O_2 ultrasensitive sensor.

2. Experimental

2.1. Chemicals

MP-11 (ca. 90% pure, sodium salt, molecular weight [MW] 1881, from equine heart cytochrome c), β-D-glucose, 4,4′-diphenylmethane diisocyanate (MDI), poly (teramethylene ether glycol) (PTMG) and dimethylol propionic acid (DMPA) were purchased from Sigma–Aldrich. Ascorbic acid, uric acid, citric acid and 30% H_2O_2 solution were obtained from Shanghai Chemical Company (Shanghai, China). These chemicals were used as received except for PTMG and DMPA. Both were pretreated as described in our previous paper (Mao et al., 2009) to remove residual water before use. All other chemicals were of analytical grade and used without further purification. A fresh solution of H_2O_2 was prepared just before each experiment. Phosphate buffered solution (PBS) with various pH values was made from mixing separate solutions of Na_2HPO_4 and NaH_2PO_4 as needed to achieve the desired pH. All solutions were prepared with double-distilled water.

2.2. Preparation of polyurethane nanoparticles

Polyurethane nanoparticles with a mean diameter of 50 nm were synthesized by an emulsion polymerization as described previously (Mao et al., 2009). Typically, the mixture of MDI and PTMG in anhydrous ethyl acetate solvent under dry nitrogen purge with 0.9 wt% dibutyltin dilaurate included as a catalyst were firstly heated to 75 °C, then the DMPA dissolved in pyrrolidinone was gradually dropped into and the mixture was reacted for about 4 h, followed by the addition of the isopropanol acting as an end-capping agent. The calculated molar ratio for MDI/DMPA/PTMG was 3.2/1/2.2. Finally, the obtained product was subsequently treated with triethylamine, and then poured into a large amount of sodium dodecyl sulfate (SDS) solution to prepare nano-sized PU particles. Furthermore, the freshly made PU-NPs were redispersed in phosphate buffered solution and purified by dialysis to remove unreacted monomers, SDS and salts.

2.3. Fabrication of PU-NP-modified electrodes

Glassy carbon electrode (GCE, 3 mm in diameter) was polished sequentially with slurries of 0.3 and 0.05 μm alumina to a mirror finish while ultrasonic cleaning in water and ethanol, respectively, for 30 s between each polishing step, and then dried at room temperature. A 4 mg/mL PU-NPs solution was prepared by dissolving PU-NPs powder in 0.1 M PBS (pH = 6.9) via 30-min ultrasonication. This solution was then stored at 4 °C until use, at which point it was sonicated again for another 10 min. To generate a MP-11-entrapped PU-NP-modified electrode (MP-11-PU-NPs/GC), the above PU-NPs solution was mixed with the same volume of 0.4 mg/mL MP-11 solution in 10 mM PBS. And then 5 μl of the mixture was evenly spread onto the surface of the pretreated GC electrode, which was then dried at ambient temperature. The control electrode (PU-NPs/GC) was fabricated similarly except that 2 mg/mL PU-NPs solution in 0.1 M PBS without adding MP-11 was used instead. If not used immediately, the modified electrodes were soaked in 10 mM PBS at 4 °C.

2.4. Apparatus and procedures

The electrochemical characterizations were carried out using a CHI 660B electrochemical workstation (CH Instruments) at room temperature, in a conventional three-electrode cell configuration, with phosphate buffer as a supporting electrolyte. A 3 mm diameter GCE, coiled Pt wire and a saturated calomel electrode (SCE) were used as working electrode support, counter and reference electrode, respectively. All the potentials were quoted with respect to SCE. Cyclic voltammetric measurements were handled in an unstirred electrochemical cell. Alternatively, the amperometric detection was performed under an applied potential of −0.42 V in a stirred cell at an optimal speed for a good single-to-noise ratio and a short response time. To remove dissolved molecular O_2, all buffered solutions were purged with nitrogen gas for at least 30 min prior to any experiment and the nitrogen atmosphere was then maintained over solution during the experiments. All the electrochemical measurements were carried out at (22 ± 1) °C.

The circular dichroism (CD) spectra both in the far-UV (185–260 nm) and Soret (340–480 nm) region were recorded with a Jasco J-715 spectropolarimeter using a 0.2 cm quartz cuvette. A data interval of 0.5 mm and a digital integration time of 0.5 s were selected. Eight scans were collected and averaged for each spectrum. The content of α-helix, β-sheet, β-turn and the random coil was calculated by the method reported in the previous work (Chang et al., 1978; Woody and Sreerama, 1999), using the SSE-338 program provided by JASCO Co.

Fourier transform infrared (FTIR) spectra were recorded on KBr disk containing about 1% sample by weight with a Nexus 670 FT-IR spectrophotometer (Nicolet Instruments Co., USA). For each sample, a total of 64 scans at a resolution of 4 cm^{-1} were collected.

Transmission Electron Microscopy (TEM) was performed with a JEOL JEM 2010 interface high-resolution TEM instrument (Japan), operating at an accelerating voltage of 120 kV.

3. Results and discussion

3.1. Physical characterization

Nano-sized PU with a homogeneous structure was successfully synthesized for the first time by the emulsion polymerization, whose chemical structure is illustrated in Scheme 1. To characterize the morphology and properties of the resulting PU-NPs, FTIR and TEM were subsequently performed, respectively. As is shown in the TEM image (Fig. 1A), the prepared PU-NPs were well-dispersed with an average hydrodynamic diameter of ca. (50.7 ± 8.3) nm. Obviously, the resulting particles were also relatively uniform in size and shape. And its long-term stability both in aqueous solution and dry state at room temperature was further confirmed in the following experiments.

The profile-view high resolution TEM image of a single PU-NPs (Fig. 1A, inset) showed that the surface of the prepared matrix for MP-11 immobilization was quite rough and kind soft with increased surface area, compared to the conductive metallic nanoparticles such as Au nanoparticles (Zanchet et al., 2000), which is beneficial to achieve higher enzyme loading causing lower detection limit and higher amperometric catalytic current to the electro-reduction of H_2O_2 as demonstrated in the following experiments.

The FTIR spectra of the PU-NPs are shown in Fig. 1B. As spectroscopic evidence, the specific absorption peaks appearing at 3440, 2940, 2860, 1637, 1543, 1223, 1110 cm^{-1}, in complete agreement with the respective component of the polymer chain (Lee et al., 1998; Mishra et al., 2010; Socrates, 2004), further proved the successful formation of PU. The absorption band at 3440 cm^{-1} was assigned to the N–H stretching vibrations of secondary amines. The two peaks between 2940 and 2860 cm^{-1} respectively corresponded to CH_2 asymmetric and symmetric vibration mainly present in soft segments. The carbonyl absorption band, C=O of the –CONH group, is known as the amide I band located at 1637 cm^{-1}, which was shifted to lower frequencies compared to the typical range around 1720–1740 cm^{-1} most probably due to the hydrogen-bond formation. And the N–H in-plane bending at 1543 cm^{-1} was termed the amide II band. Peaks at 1223, 1110 cm^{-1} presented the C–O stretching of esters and ethers, respectively.

The CD spectra of dissolved MP-11 in the absence and presence of PU-NPs were examined within the intrinsic absorption region to characterize the effect of the added PU-NPs on the structure of MP-11. As shown in Fig. 2A, curve a, the MP-11 exhibited a positive peak at ca. 192 nm, negative band around 220 nm and a slight shoulder at ca. 200 nm. The positive maximum at ca. 192 nm is corresponding to π–π^* amid transition, whereas the negative minimum around 220 nm is predominantly a result of n–π^* amid transition. Both suggest the existence of two distinct structural organizations of the polypeptide chain, namely α-helical and β-conformation. In addition, the small shoulder around 200 nm is attributed to randomly coiled peptides. When MP-11 was mixed with PU-NPs, there was no remarkable variations occurring in the shape and position of the characteristic ellipticity bands for MP-11 (Fig. 2A, curve b), which was further confirmed by the calculated content of each secondary structure including α-helical, β-turn and random coil, listed in the inset table of Fig. 2A. Furthermore, in the Soret absorption region, the CD spectra of the MP-11-NPs mixture (Fig. 2B, curve b), become almost the same as that of the MP-11 solution, except for a slight decrease in the molar ellipticity with a concurrent very small red shift in the position of the typical Soret band at ca. 400 nm, indicating the reasonable interaction between PU-NPs and MP-11. These findings demonstrated that the existing of PU-NPs induced no significant conformational alterations of both the polypeptide chain and the prosthetic group to MP-11, which is in good agreement with the next presented electrochemical results.

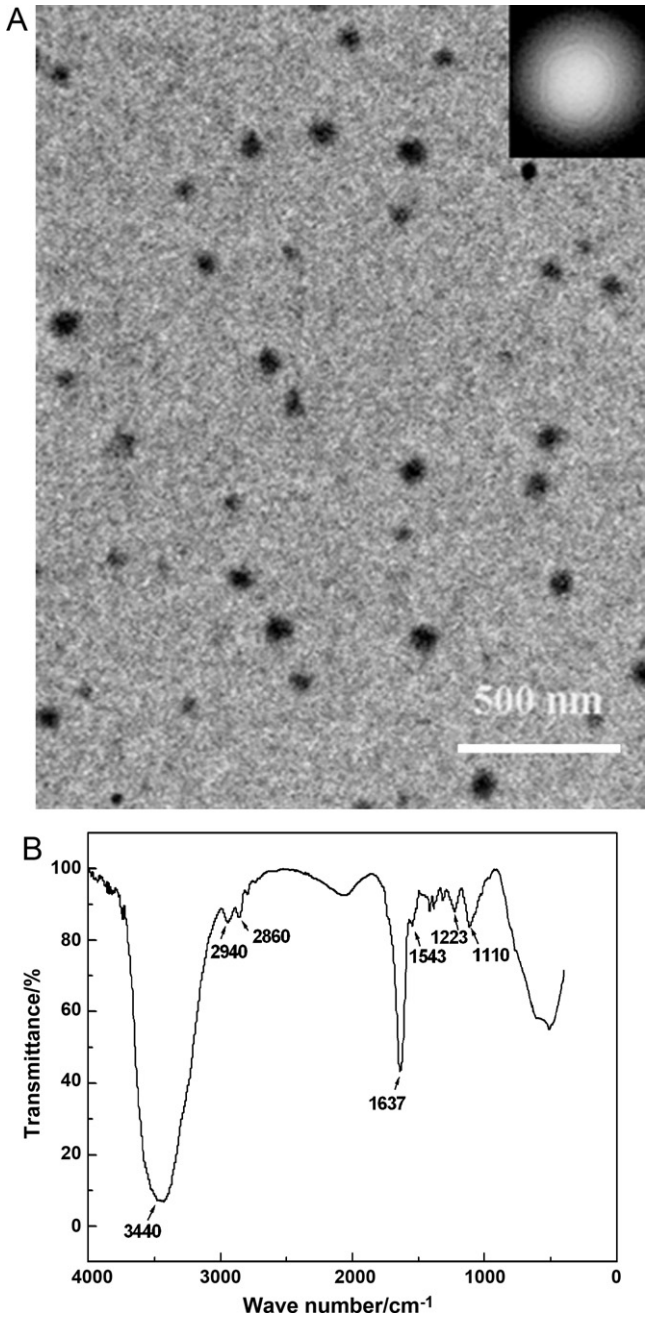

Fig. 1. (A) TEM image and (B) FTIR spectra of PU-NPs prepared by an emulsion polymerization with small diameter around 50 nm and long-term stability. Inset in A: high resolution TEM image of a single PU-NPs.

3.2. Electrochemical reduction of H_2O_2 at the MP-11-PU-NPs/GC electrode

MP-11 is an oligopeptide including 11 amino acids with an iron protoporphyrin IX as the redox-active center, which is often used as a catalyst for the construction of H_2O_2 biosensor. The electrochemical activity of MP-11 incorporated in the nanostructured PU was

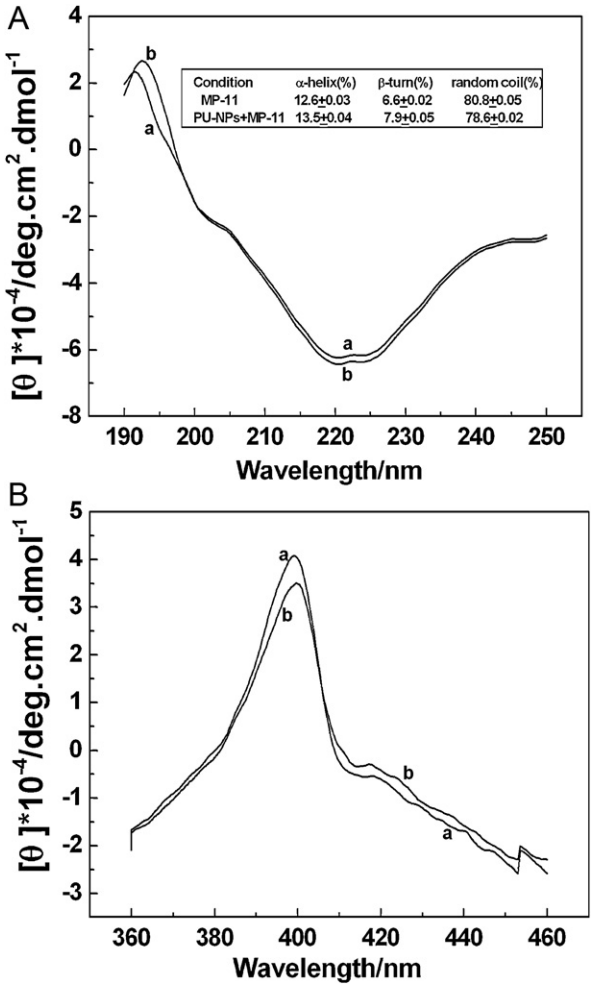

Fig. 2. The CD spectra of dissolved MP-11 at the concentration of 1.38 μM with (a) 0, (b) 10 mg/mL PU-NPs in the wavelength region of (A) 190–250 nm and (B) 360–460 nm. Inset table in A: calculated secondary structure content of 1.38 μM MP-11 solution with and without added 10 mg/mL PU-NPs.

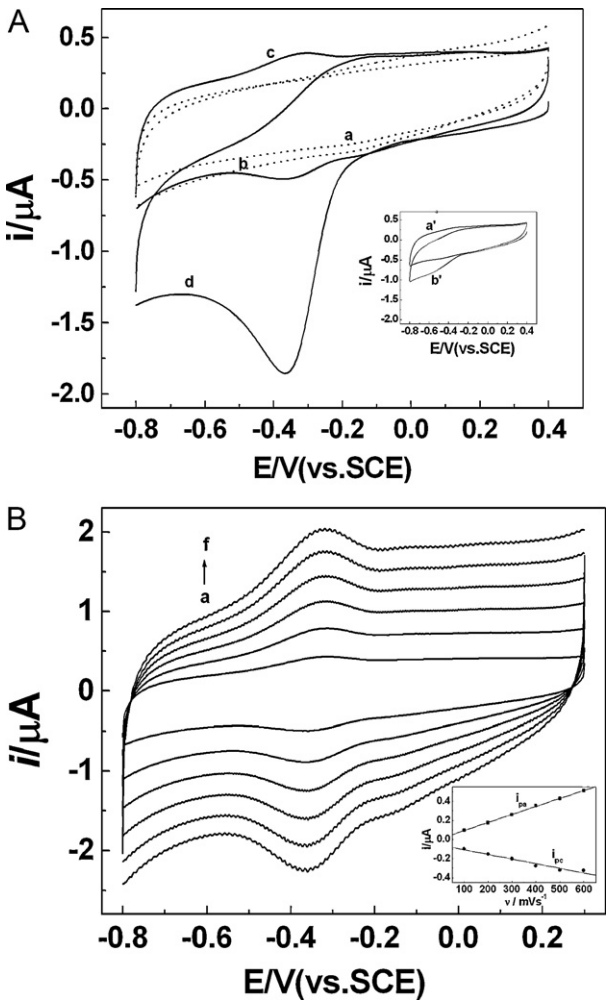

Fig. 3. (A) Cyclic voltammograms of PU-NPs/GCE (a, b, dot line) and MP-11-PU-NPs/GCE (c, d, solid line) in 0.1 M PBS with (b, d) and without (a, c) 0.047 mM H_2O_2 at 100 mV s^{-1}. Inset: CVs of PU film modified GCE at the same condition as Curve c and d. (B) Cyclic voltammograms of MP-11-PU-NPs/GCE in 0.1 M PBS at various scan rates of (a) 100, (b) 200, (c) 300, (d) 400, (e) 500 and (f) 600 mV s^{-1}. Inset: plots of redox peak currents versus scan rates.

investigated. Fig. 3A presents the cyclic voltammograms of a MP-11-PU-NP-modified GCE (curves c and d) relative to the control of PU-NP-modified GCE (curves a and b). No electrochemical response was observed for the PU-NP-modified GCE control in 0.1 M PBS, pH 6.9, at 100 mV s^{-1} in the absence of dissolved H_2O_2 within the potential range of −0.8 to +0.4 V. By contrast, the PU-NP-modified GCE with immobilized MP-11 showed two distinct and nearly symmetric redox peaks. The anodic peak potential (E_{pa}) and cathodic peak potential (E_{pc}) are located at −0.338 and −0.348 V, respectively, against reference. Obviously, the presence of the pair of redox peaks is attributed to an electrochemical reaction of the physically attached MP-11 between MP-Fe(III) and MP-Fe(II), via the promotion of PU-NPs, which provides a three-dimensional stage for the protein immobilization. To verify this, an additional control experiment was performed whereby the MP-11 was immobilized to a thin layer of PU film that had been drop-cast onto the surface of the GCE. The CV result, shown in the inset of Fig. 3A, revealed extremely small and relatively irreversible voltammetric response, suggesting that the redox peaks observed for the MP-11 (Fig. 3A, curve c) was due to the electron transfer between the MP-11 and GCE, facilitated by the nano-sized PU.

The separation of peak potentials, ΔE_p, for the anodic and cathodic peaks was calculated to be 10 mV, which is much smaller than those in the literature (Astuti et al., 2011; Zhou et al., 2010) and probably the smallest one compared to that found in the literature so far. This suggests that the preferred orientation of immobilized MP-11 on the surface of the GCE was obtained in the presence of PU-NPs, which induce much effective electron transfer from the iron protoporphyrin IX of MP-11 to the GCE. Since the cathodic peak current (i_{pc}) was almost equal to the anodic peak current (i_{pa}), the MP-11-immobilized PU-NPs appears to undergo a quasi-reversible electrochemical reaction. Its formal potential (defined as the average of the anodic and cathodic peak potentials), $E^{\circ\prime}$, is–0.343 V at a scan rate of 100 mV s^{-1}, which is more positive than the result of −0.35 V (vs. Ag/AgCl) on {Chitosan/MWNT/Chitosan}$_n$ multilayer (Xu et al., 2005) and negative than that obtained for MP-11 assembled on a GC electrode or Au electrode (Ruzgas et al., 1999). This suggests that most biomolecules preserved their original structure even after being entrapped in the PU-NPs, which is in good agreement with the result from the CD spectroscopic characterization. The negative shift of the peak potentials is presumably attributed to the presence of the PU-NPs in low conductivity, which can stabilize the oxidized form of MP-11.

Fig. 3B shows the cyclic voltammograms of the MP-11-entrapped PU-NP-modified GCE in 0.1 M PBS (pH = 6.9) at various scan rates (v). From the integration of the oxidation peak of the MP-11-PU-NPs/GC electrode at scan rates of 100–800 mV s^{-1},

an average surface coverage (Γ) of MP-11 is calculated to be $(1.48 \pm 0.01) \times 10^{-11}$ mol/cm^2, by assuming a one-electron reaction, which is in the same order as that of MP-11 immobilized on SWNTs (Gooding et al., 2003). Compared with the final amount of MP-11 loading on the surface of PU-NPs, which was calculated by subtracting the leached amount in washing solution from the one initial added, approximate 9% of the immobilized enzyme retained its electrochemical activity. The values of E_{pa} and E_{pc} keep almost invariable at the scan rate ranging from 100 up to 2500 mV s^{-1}, yielding a formal potential $E^{\circ\prime} = -(0.345 \pm 0.002)$ V across all scan rates mentioned above. In addition, i_{pa} and i_{pc} were found to be linearly proportional to the scan rate (Fig. 3B, inset), suggesting that the reaction is a surface-controlled process, commonly observed in systems employing immobilized enzymes. From the measured ΔE_p, an apparent heterogeneous electron-transfer rate constant, $k_s = (19 \pm 5.7)$ s^{-1}, was calculated using the method developed by Laviron for a surface-controlled electrochemical reaction. The value of k_s is higher than those reported previously, 13 ± 1 s^{-1} for MP-11 anchored on cystamine monolayer modified electrode (Lötzbeyer et al., 1996; Willner et al., 1998), 9.4 s^{-1} for MP-11 on 3-mercaptopropionic acid monolayer modified electrode (Gooding et al., 2003), 1.27 s^{-1} on MWNTs with attached gold nanoparticles (Liu et al., 2005) and (2.2 ± 0.2) s^{-1} on SnO_2-poly-L-lysine electrode (Astuti et al., 2011) which, to some degree, may indicate a reasonably fast electron transfer between the immobilized MP-11 and the supporting electrode.

Upon addition of 0.047 mM H_2O_2, the shape of cyclic voltammogram of the MP-11-PU-NPs/GC electrode changes significantly and is characterized by a large cathodic peak starting at ca. −0.127 V (Fig. 3A, curve d), attributed to the electrocatalytical reduction of H_2O_2. Controlled experimental results indicated that no catalytic current was observed at the bare GC or PU-NPs/GC electrode (Fig. 3A, curve b) in the presence of H_2O_2, whereas at the MP-11 modified PU-film/GC electrode, the response to H_2O_2 was quite small with a ca. 20 mV negative shift in the onset potential (Fig. 3A, inset, curve b′). These results indicated that MP-11 retains its bioelectrocatalytic activity after being immobilized on the surface of PU-NPs and further confirmed that the immobilized MP-11 still remained its essential secondary structure as proved spectrophotometrically.

Fig. 4A shows the cyclic voltammograms of the MP-11-PU-NPs/GC electrode in 0.1 M PBS (pH 6.9) containing 0.047 mM H_2O_2 at various scan rates. With the increase in the scan rate, the catalytical current moves to the higher value, whereas the peak potential shifts slightly in the negative direction. The obtained peak current is found to be proportional to the square root of scan rate, $v^{1/2}$ (Fig. 4A, inset), suggesting that the electrocatalytic reaction is controlled by the diffusion of H_2O_2 in solution.

Furthermore, the reduction current of the MP-11-PU-NPs/GC electrode has a positive correlation with the concentration of H_2O_2, which is the general feature of electrocatalytic reactions for the application of substrate sensing.

3.3. Analytical performance of the MP-11-PU-NPs/GC electrode

Under optimized conditions the typical current–time response showed a good analytical performance. Fig. 4B displays the amperometric response of the MP-11-PU-NPs/GC electrode at a poised potential of −420 mV to the successive step changes of H_2O_2 concentration in 0.1 M PBS (pH = 6.9, N_2-saturated).

It is well known that the applied potential is a crucial parameter for sensitive detection of a substrate via an amperometric biosensor. The optimal working potential of −0.42 V for the prepared biosensor was selected base on a series of experiments, which condition was set the same as that in the following interference experiments. The experimental results showed that the electrocatalytic cathodic current of H_2O_2 kept on rising with the decrease of the potential from 0 to −0.4 V, then leveling off obviously after the potential lower than −0.42 V. For the interferents' disturbance, there is no significant influence on the amperometric detection of H_2O_2 at the potential of −0.42 V, though the concentration of each interferent was two times higher than that of added H_2O_2, whereas the disturbance current goes up when the poised potential greater than −0.3 V (figure not shown). Therefore, the potential of −0.42 V was employed as a suitable potential to amperometric detection of H_2O_2.

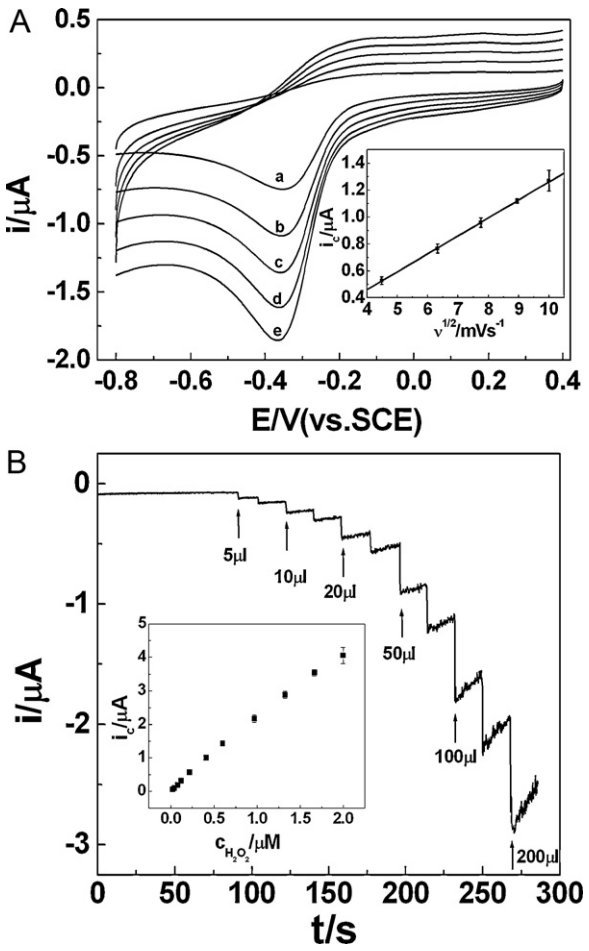

Fig. 4. (A) Cyclic voltammograms of MP-11-PU-NPs/GCE in 0.1 M PBS with 0.047 mM H_2O_2 at various scan rates of (a) 20, (b) 40, (c) 60, (d) 80 and (e) 100 mV s^{-1}. Inset: plots of reduction peak currents versus the square root of the scan rates with average data taken from four different and freshly prepared electrodes. (B) Amperometric response of the MP-11-PU-NPs/GC electrode by successive addition of different volume of 0.2 μM H_2O_2 to 5 mL of N_2-saturated 0.1 M PBS, pH = 6.9, under stirring at −0.42 V (vs. SCE). Inset: plot of response currents versus the corresponding concentration of H_2O_2. The relative standard deviations of each response current at different concentration from 0.02 to 2.0 μM were 0.002, 0.003, 0.007, 0.009, 0.014, 0.071, 0.028, 0.11, 0.1, 0.1, 0.24 μA, respectively, base on data taken from six different and freshly prepared electrodes.

Following the addition of H_2O_2, the current response increased and reached a maximum value within (1.32 ± 0.44) s. The response time was defined as the time required reaching 95% of the maximum steady-state current and the value showed above was the average result from five freshly made different electrodes. The electrode linearly responds to H_2O_2 at lower concentration from 0.02 to 1.3 μM ($R = 0.998$), whereas at higher concentration, the current levels off as expected for Michaelis–Menten type enzyme (inset in Fig. 4B). It is noted that the dynamic linear range in our scheme is quite desirable especially to the determination of

Table 1
Evaluation of possible interferents to H_2O_2 biosensors expressed as percentage of H_2O_2 response current.

Potential interfering substance	Current ratio
H_2O_2	1.00
Glucose	0.92
Citric acid	0.93
Uric acid	0.94
Ascorbic acid	0.91

H_2O_2 at ultralow concentration for samples from the physiological system since as an example, hydrogen peroxide released from neutrophils in exhaled breath condensate (EBC), which concentration was in the range of 0.1–1 μM (Svensson et al., 2004). The apparent Michaelis–Menten constant (K_M^{app}) was estimated to be 1.9 μM from the Lineweaver–Burk plot (Kamin and Wilson, 1980). This K_M^{app} value was much smaller than those of 2.0 mM for H_2O_2 biosensors based on sol–gel immobilized HRP (Tripathi et al., 2006), 2.4 mM with MWNT-modified MP-11 (Wang et al., 2005a), 7.6 mM based on sol–gel gold nanotubes (Delvaux et al., 2004), 3.4 mM on MWNTs film-modified Pt microelectrodes (Wang et al., 2005b) and 0.54 mM on chitosan–graphene nanocomposite (Zhou et al., 2010). Low K_M^{app} value indicated that the enzyme immobilized on the PU-NPs retained its activity with a low diffusion barrier. Within the linear response range, the calculated sensitivity was $(29.6 \pm 0.59)\,\mu A\,\mu M^{-1}\,cm^{-2}$. The apparent surface area of the electrode was estimated using the method reported elsewhere (Sun et al., 2004). The limit of detection was estimated to be as low as ca. 0.01 nM (at S/N = 3), which is extended by at least ca. 3 orders of magnitude below other reported values (Behera and Raj, 2007), indicating a marked improvement for direct H_2O_2 detection via immobilized redox protein.

More performance properties of the prepared H_2O_2 biosensor based on immobilized MP-11 via PU-NPs were further investigated. The reproducibility of the prepared biosensor to H_2O_2 at the concentration of 0.047 mM has been estimated by four different and freshly prepared electrodes. The relative standard deviation (R.S.D.) in the response for the sensing of H_2O_2 was calculated to be ca. 3%, yielding a reasonable reproducible result in the construction of the electrode. The stability of the electrode was examined by measuring the CV peak current in N_2-saturated PBS using the same electrode over a quite long period of time. It should be mentioned here that the response to the reduction of H_2O_2 will not change if the anodic or cathodic current for the direct electron transfer of entrapped MP-11 keeps the same value as demonstrated in our experiments. When the electrode was not in use, it was stored in buffer at 4 °C and the CV was recorded at various interval lengths (figure not shown). The response slowly decreased to ca. 95% of its original response at the initial 15 days, and tends to be practically constant within the next 20 days. The decrease in CV peak current was attributed to the leakage of the immobilized enzyme on PU-NP modified layer. This can be further demonstrated by the fact that the mixture of MP-11-PU-NPs in solution for the construction of MP-11-modified electrodes remained its bioactivity without any discernable decrease even after stored in a freezer for more than 5 months. The stability especially the storage stability is much higher than those reported in the literature so far. It can be contributed to the benign microenvironment for the redox protein provided by nano-sized PU with good biocompatability, large surface-to-volume ratio and the increased surface activity.

The analytical performance of the developed H_2O_2 biosensor in the presence of possible interferents such as glucose, citric acid, uric acid and ascorbic acid was investigated. Table 1 shows the amperometric response of each interfering substance at 10 μM, which was successively added following H_2O_2 at 5 μM, was expressed as relative value with respect to that of H_2O_2. The concentration of the interferent was one or two times greater than that in real biological systems. The results indicate that glucose, citric acid, uric acid, and ascorbic acid did not cause enough interference in the amperometric measurement, though the amount of the first added H_2O_2 was half of those following interferents, which is similar to that reported in the literature (Wan et al., 2009). Further experiments showed that the existing interferents had negligible effect on the response time to amperometric detection of H_2O_2 via the prepared biosensor, which value in the absence and presence of glucose, citric acid, uric acid and ascorbic acid was (1.26 ± 0.38) s, (0.97 ± 0.25) s, (0.89 ± 0.26) s, (2.58 ± 0.52) s and (0.49 ± 0.08) s, respectively. Therefore the concentration of H_2O_2 can be monitored without major interference through our established sensing scheme.

4. Conclusion

Evidence of the direct electrical communication between the underlying electrode GCE and redox protein MP-11, attached to the nano-sized polyurethane, was observed. The high rate of electron transfer through the PU-NPs to MP-11 was clearly demonstrated by the similar rate constant as those in the literature. Further experimental results revealed that the developed amperometric biosensor for hydrogen peroxide determination exhibited significantly low detection limit, great analytical sensitivity and relative fast response with long-term stability. The PU-NPs with attractive properties as a promising matrix for enzyme immobilization have paved the way for the construction of ultrasensitive amperometric biosensors with a wide range of applications.

Acknowledgements

The authors thank the financial support from the “863” Project (Grant No. 2007AA05Z154), the National Science Foundation of the Jiangsu Higher Education Institutions of China (Grant Nos. 10KJD150004, 08KJA430003), the National Natural Science Foundation of China (Grant No. 20874047), the National Science Foundation for Young Scholars of China (Grant No. 21005039), the Project Sponsored by the Scientific Research Foundation for the Returned Overseas Chinese Scholars by State Education Ministry (2010609) and Nanjing Normal University, the Project Funded by the Priority Academic Program Development (PAPD) of Jiangsu Higher Education Institutions.

References

Astuti, Y., Topoglidis, E., Durrant, J.R., 2011. Anal. Chim. Acta 686, 126–132.
Behera, S., Raj, C.R., 2007. Biosens. Bioelectron. 23, 556–561.
Bil, M., Ryszkowska, J., Wozniak, P., Kurzydlowski, K.J., Lewandowska-Szumiel, M., 2010. Acta Biomater. 6, 2501–2510.
Chang, C., Wu, C., Yang, J., 1978. Anal. Biochem. 91, 13–31.
Chen, S.H., Yuan, R., Chai, Y.Q., Zhang, L.Y., Wang, N., Li, X.L., 2007. Biosens. Bioelectron. 22, 1268–1274.
Deka, H., Karak, N., Kalita, R.D., Buragohain, A.K., 2010. Carbon 48, 2013–2022.
Delvaux, M., Walcarius, A., Demoustier-Champagne, S., 2004. Anal. Chim. Acta 525, 221–230.
Dickinson, B.C., Chang, C.J., 2008. J. Am. Chem. Soc. 130, 9638–9639.
Gooding, J.J., Wibowo, R., Liu, J.Q., Yang, W.R., Losic, D., Orbons, S., Mearns, F.J., Shapter, J.G., Hibbert, D.B., 2003. J. Am. Chem. Soc. 125, 9006–9007.
Hood, M.A., Wang, B.B., Sands, J.M., La Scala, J.J., Beyer, F.L., Li, C.Y., 2010. Polymer 51, 2191–2198.
Jiang, X.E., Jiang, J.G., Jin, Y.D., Wang, E.K., Dong, S.J., 2005. Biomacromolecules 6, 46–53.
Kamin, R., Wilson, G., 1980. Anal. Chem. 52, 1198–1205.
Katz, E., Willner, I., 1996. J. Electroanal. Chem. 418, 67–72.
Katz, E., Willner, I., 1997. Langmuir 13, 3364–3373.
Klassen, N., Marchington, D., McGowan, H., 1994. Anal. Chem. 66, 2921–2925.
Koepsel, R.R., Russell, A.J., 2003. Biomacromolecules 4, 850–855.
Kulys, J., Tetianec, L., 2006. Sens. Actuators B: Chem. 113, 755–759.
Lee, D., Lee, J., Koide, N., Akiyama, E., Uryu, T., 1998. Macromolecules 31, 975–981.
Liu, S.Q., Lin, B.P., Yang, X.D., Zhang, Q.Q., 2007. J. Phys. Chem. B 111, 1182–1188.

Liu, Y., Wang, M.K., Zhao, F., Guo, Z.H., Chen, H.J., Dong, S.J., 2005. J. Electroanal. Chem. 581, 1–10.
Lo, L.C., Chu, C.Y., 2003. Chem. Commun. 21, 2728–2729.
Lötzbeyer, T., Schuhmann, W., Schmidt, H., 1996. Sens. Actuators B: Chem. 33, 50–54.
Lyon, J.L., Stevenson, K.J., 2006. Anal. Chem. 78, 8518–8525.
Mao, C., Jiang, L., Luo, W., Liu, H., Bao, J., Huang, X., Shen, J., 2009. Macromolecules 42, 9366–9368.
Mazzei, F., Favero, G., Frasconi, M., Tata, A., Tuccitto, N., Licciardello, A., Pepi, F., 2008. Anal. Chem. 80, 5937–5944.
Mir, M., Jenkins, A.T.A., Katakis, I., 2008. Electrochem. Commun. 10, 1533–1536.
Mishra, A., Aswal, V.K., Maiti, P., 2010. J. Phys. Chem. B 114, 5292–5300.
Munge, B.S., Dowd, R.S., Krause, C.E., Millord, L.N., 2009. Electroanalysis 21, 2241–2248.
Niethammer, P., Grabher, C., Look, A.T., Mitchison, T.J., 2009. Nature 459, 996–999.
Patolsky, F., Gabriel, T., Willner, I., 1999. J. Electroanal. Chem. 479, 69–73.
Phadtare, S., Kumar, A., Vinod, V.P., Dash, C., Palaskar, D.V., Rao, M., Shukla, P.G., Sivaram, S., Sastry, M., 2003. Chem. Mater. 15, 1944–1949.
Poole, L.B., Nelson, K.J., 2008. Curr. Opin. Chem. Biol. 12, 18–24.
Rhee, S.G., 2006. Science 312, 1882–1883.
Ruzgas, T., Gaigalas, A., Gorton, L., 1999. J. Electroanal. Chem. 469, 123–131.
Schraufstatter, I., Hyslop, P., Hinshaw, D., Spragg, R., Sklar, L., Cochrane, C., 1986. Proc. Natl. Acad. Sci. U.S.A. 83, 4908.
Shu, X.H., Chen, Y., Yuan, H.Y., Gao, S.F., Xiao, D., 2007. Anal. Chem. 79, 3695–3702.
Socrates, G., 2004. Infrared and Raman Characteristic Group Frequencies: Tables and Charts, 3rd ed. John Wiley & Sons Inc., Chichester, UK.
Sun, D.M., Cai, C.X., Li, X.G., Xing, W., Lu, T.H., 2004. J. Electroanal. Chem. 566, 415–421.
Svensson, S., Olin, A.C., Larstad, M., Ljungkvist, G., Toren, K., 2004. J. Chromatogr. B 809, 199–203.
Tripathi, V.S., Kandimalla, V.B., Ju, H.X., 2006. Biosens. Bioelectron. 21, 1529–1535.
Wan, J., Bi, J.L., Du, P., Zhang, S.S., 2009. Anal. Biochem. 386, 256–261.
Wang, D.A., Ji, J., Sun, Y.H., Shen, J.C., Feng, L.X., Elisseeff, J.H., 2002. Biomacromolecules 3, 1286–1295.
Wang, M.K., Shen, Y., Liu, Y., Wang, T., Zhao, F., Liu, B.F., Dong, S.J., 2005a. J. Electroanal. Chem. 578, 121–127.
Wang, M.K., Zhao, F., Liu, Y., Dong, S.J., 2005b. Biosens. Bioelectron. 21, 159–166.
Willner, I., Arad, G., Katz, E., 1998. Bioelectrochem. Bioenerg. 44, 209–214.
Wilson, G.S., Hu, Y.B., 2000. Chem. Rev. 100, 2693–2704.
Woody, R., Sreerama, N., 1999. J. Chem. Phys. 111, 2844.
Xu, D., Wu, K., Zhang, Q.H., Hu, H.Y., Xi, K., Chen, Q.M., Yu, X.H., Chen, J.N., Jia, X.D., 2010. Polymer 51, 1926–1933.
Xu, Z., Gao, N., Chen, H., Dong, S.J., 2005. Langmuir 21, 10808–10813.
Yu, X., Chattopadhyay, D., Galeska, I., Papadimitrakopoulos, F., Rusling, J.F., 2003. Electrochem. Commun. 5, 408–411.
Yuan, J., Shiller, A., 1999. Anal. Chem. 71, 1975–1980.
Zanchet, D., Hall, B.D., Ugarte, D., 2000. J. Phys. Chem. B 104, 11013–11018.
Zhou, Y., Liu, S., Jiang, H.J., Yang, H., Chen, H.Y., 2010. Electroanalysis 22, 1323–1328.